JOURNAL OF PROPULSION AND POWER
Vol. 16, No. 6, November–December 2000

Multicomponent-Fuel Film-Vaporization Model for Multidimensional Computations

Yangbing Zeng* and Chia-Fon Lee†
University of Illinois at Urbana–Champaign, Urbana, Illinois 61801

A multicomponent-fuel film-vaporization model is developed to be used in multidimensional spray and combustion computations. For the gas phase the vaporization rate was evaluated using the turbulent boundary-layer assumption and the Prandtl mixing-length theory. A third-order polynomial was used to model the temperature and species concentration profiles within the liquid film in order to predict accurate surface temperature and surface mass fractions, which are crucial to evaluating the species vaporization rates. By this approach the governing equations for the film were reduced to a set of ordinary differential equations. The new model offers a significant reduction in computational cost and sufficient accuracy compared to solving the governing equations for the film directly. The new model was verified against exact numerical solutions with excellent agreement for several cases concerning the vaporization process of a film on a flat plate. The results were also compared with the solutions obtained using an infinite-diffusion model. The new model predicted the vaporization history more accurately than the infinite-diffusion model. Finally, the new model was applied to study the film evolution for a spray/wall impingement case, and physical insight was gained from the study.

Nomenclature

B = mass-transfer number
Cp = heat capacity
C_μ = turbulent model constant, 0.09
D = mass-diffusion coefficient
E = internal energy
H_Y = overall mass transfer coefficient of the film
h_t = heat-transfer coefficient
h_v = latent heat of vaporization
K = turbulent kinetic energy
k = heat conductivity
Pr = Prantdl number
q = heat flux
Sc = Schmidt number
T = temperature
t = time
V = velocity
Y = mass fraction
y = distance from the wall
y^+ = nondimensional distance from the wall
y^* = normalized y coordinate
α = thermal diffusivity
Γ = mass-diffusion coefficient
δ = film height
θ = nondimensional temperature
κ = Karmann's constant, 0.433
μ = viscosity
ρ = density
τ = nondimensional time
ω = vaporization rate

Subscripts

g = gas phase
i = species component
L = laminar
ℓ = liquid phase
m = average value
o = initial value
s = surface value
T = turbulent
∞ = ambient value

Received 22 February 1999; revision received 27 July 1999; accepted for publication 30 July 1999.

*Graduate Student, Department of Mechanical and Industrial Engineering.
†Assistant Professor, Department of Mechanical and Industrial Engineering.

I. Introduction

LIQUID-FILM phenomena are important in the study and design of internal combustion (gasoline and Diesel) engines. Significant amounts of droplets hit the walls of the intake port or the cylinder after they leave the injector. Based on the injection conditions, the droplets rebound, splash, or convert into liquid films on the wall. Zeng and Lee[1] found that nearly 80% of the fuel mass deposited on the wall and became wall films for closed-valve injection in computations of cold starting of a port-injected spark-ignition engine. Open-valve injection tends to produce less film mass deposition in the intake port; however, this film mass still accounts for nearly 50% of the total fuel mass. Film formation and evolution have significant effects on engine emission. They influence the mixture quality of the fuel vapor and the oxidizer, which in turn control the combustion efficiency, pollutant formation, and heat transfer to the wall. It is believed that incomplete vaporization of liquid fuel film results in high hydrocarbon emissions and soot formation.[2,3] For port-injected spark-ignition engines experiments show that up to 80% of the total hydrocarbon emission is generated during the first few minutes of cold starting.[4] The primary reason is that most fuel droplets become liquid films on the cold wall where the vaporization rate of the films is much slower than that of the droplets caused by a smaller surface-to-volume ratio. Therefore, understanding film formation and evolution is of great practical significance. It will help optimize engine design to meet the increasingly stringent emission regulations.

Although many research efforts have been made to understand the liquid-film phenomena (e.g., wall film dynamics,[5–8] impingement,[9,10] and vaporization[11–17]), multicomponent film vaporization has not been extensively studied. Particle methods[5,6] and continuous methods[7,8] have been proposed to represent films. Particle methods represent the film mass by a group of particles and solve the film particle movement using the Lagrangian description of motion. Particle methods are superior to continuous methods for modeling the irregular shape and size of the films resulting from spray impingement and surface tension effects. O'Rourke and Amsden[5] and Amsden[6] developed a comprehensive model for film formation and evolution

in port-injected engines based on a particle method. A modified wall function was used to account for the effects of film vaporization on mass, momentum, and thermal diffusive transport. Bai and Gosman[7] developed a model to evaluate the vaporization rate using semi-empirical correlations involving the mass-transfer coefficient and the Sherwood number. This model required the definitions of a characteristic film height and a characteristic longitudinal length, which are difficult to determine for some applications. One important advantage of these two models[5–7] over conventional methods, which use continuity principle of mass flux to calculate the vaporization rate, is that the grid resolution near the wall does not have to be very fine. This makes these two models feasible for engine computations, especially for those requiring moving-grid operations. However, these models are limited to single-component films, which is a severe limitation because most practical fuels are multicomponent in nature. The computations of Baumann and Thiele[11,12] show that film composition significantly affects the mass and heat-transfer behaviors. Even adding a small amount of a second component can result in significant changes in the heat and mass transfer.

The major complexity associated with film-vaporization modeling is how to evaluate accurately the surface values of temperature and mass fractions, which are key variables controlling the evaporation rate. When the film is being heated by the wall or the ambient gas, the temperature distribution in the film is nonuniform during most of the lifetime of the film because of the thermal diffusion resistance. The multicomponent nature of practical fuels brings additional complexity. When the film-vaporization rate is high, the great differences in vaporization rates among components result in nonuniformity and transient variation of the composition of the film because vaporization occurs only on the surface. The component mass inside cannot reach the surface quickly enough because of the mass-diffusion resistance. Therefore, it is not generally acceptable to assume that the temperature and mass-fraction profiles are uniform. Consequently, it is necessary to solve the equations describing their temporal and spatial variations in order to model film evaporation accurately. With currently available computational ability, however, it is impractical to use tens of grids for each film particle to obtain accurate numerical solutions because thousands of particles would be necessary in a typical multidimensional computation with the particle representation of the film.[5] Appropriate predictive modeling is necessary. The existing models are either too time consuming to be applied in multidimensional spray computations or too simplistic to represent the necessary physics accurately. O'Rourke and Amsden[5] assumed that the temperature distribution inside the film is piecewise linear and the average temperature is located exactly at the half height of the film. Foucart et al.[8] used a parabolic temperature distribution. Baumann and Thiele[11] assumed a uniform profile for the mass fraction. The accuracy of these models depends on the ratio of the transient times of thermal and mass diffusions to the film lifetime. When the thermal and mass transient time of the film is comparable to its lifetime, their accuracy will decrease dramatically. Because the liquid Prandtl number and the Lewis number are typically on the order of 10, the characteristic heat conduction and mass diffusion-times are much longer than viscous transport time and even as long as the film lifetime. This is shown by scale analysis in the Appendix.

In the other extreme of modeling, Shembharkar and Pai[14] assumed that the flow in films is quasi-one-dimensional Couette flow, which requires the discretization of the thin film into tens of layers in order to obtain a grid-independent solution. This represents a tremendous computational load. Bai and Gosman[7] used a third-order polynomial to model the velocity and temperature profiles and hence simplified the boundary-layer equations for the film from a three-dimensional form to a two-dimensional form by the integral approach. For the temperature profile they used a polynomial with only one free coefficient serving as the shape factor. However, they did not address multicomponent effects. In fact, as far as we know currently, the multicomponent film vaporization models suitable for multidimensional spray simulation are very rare in the literature.

A new model for multicomponent film vaporization is presented in this paper. The vaporization formula proposed by O'Rourke and Amsden[5] and Amsden[6] was extensively modified to include multicomponent-fuel effects. A third-order polynomial was used to model the temperature and mass fraction profiles, which reduced the governing equations for the temperature and mass fractions inside the film to a set of ordinary differential equations. When compared to directly solving the governing equations for the film, the new model has a much lower computational cost with sufficient accuracy. The new multicomponent model was incorporated into a modified version[17] of the KIVA-3V (Ref. 6) code and then used to simulate the vaporization process of a film on a semi-infinite flat plate. The results were compared with an exact solution and a solution obtained using an infinite-diffusion model for multicomponent-film vaporization.[17] The infinite-diffusion model is a modification of the original O'Rourke and Amsden model.[5,6] For the mass fractions a uniform distribution is used, and for temperature, however, a piecewise linear distribution is used as in the original O'Rourke and Amsden model. The performance of the new model was also evaluated by the computation of a solid-cone spray impinging against a wall.

The rest of this paper is organized as follows. A brief overview of the KIVA-3V code will be given first, followed by a description of the gas-phase submodel for evaluating the vaporization rate, and by the derivation of the liquid-phase submodel for solving the surface temperature and mass fractions. The numerical methods involved in the model will also be given. Finally, the results and discussions will be presented for the two sets of testing computations.

II. Mathematical Models and Numerical Methods

A. General Overview of the KIVA-3V Code

KIVA-3V (Ref. 6) is a comprehensive multidimensional CFD code. The flowfield of the gas phase is obtained by solving the Reynolds-averaged Navier–Stokes equations coupled with the renormalization group k-ε turbulence model.[6] Combustion models and spray models are included in the code to account for combustion, spray atomization, breakup, and collision. The spray is represented by a particle method. The interaction of the spray and the gas flow is accounted for through coupling source terms in the governing equations. A moving-grid method is used to trace the valve and piston movement. The code has been extensively used in engine computations. The original KIVA-3V code is limited to single-component fuel. Extended efforts have been made to model multicomponent effects of sprays.[17–19] As for films, a multicomponent film vaporization model is developed in this paper and described in the following two sections.

B. Description of the Gas-Phase Submodel

The structure of the turbulent boundary-layer above the vaporizing film is different from that without vaporization because of the gas velocity normal to the wall induced by the film vaporization. This gas velocity tends to decrease the diffusive transport of mass, momentum, and energy from the gas to the film. Recently O'Rourke and Amsden[5] proposed a formula to account for this effect based on the boundary-layer equations and the Prandtl mixing-length theory. However, their formula for evaluating the film vaporization rate is limited to the single-component film. This formula was extended to include multicomponent effects by the following derivations.

The gas flow adjacent to the liquid film is assumed to be one-dimensional and in quasi-steady state. Then, for the mass fraction the following equation and boundary conditions are satisfied in this region:

$$\omega \frac{\mathrm{d}Y_i}{\mathrm{d}y} - \frac{\mathrm{d}}{\mathrm{d}y}\left(\rho D_i \frac{\mathrm{d}Y_i}{\mathrm{d}y}\right) = 0$$

$$Y_i(y=0) = Y_{\mathrm{is}},\ Y_i(y=y_\infty) = Y_{i\infty} \tag{1}$$

where ω is the total vaporization rate and y_∞ is taken as the distance of the computational cell adjacent to the film from the film surface.

Beyond this region the full Navier–Stokes equation is applied. The integration of Eq. (1) yields

$$\frac{\omega}{\rho D_i}\,\mathrm{d}y = \frac{1}{Y_i - \omega_i/\omega}\,\mathrm{d}Y_i \tag{2}$$

The intergration of the preceding equation will give the expression for the total vaporization rate

$$\omega = \left(\int_0^{y_\infty} \frac{1}{\rho D_i}\,\mathrm{d}y\right)^{-1} \ln\left(\frac{\omega_i/\omega - Y_{i\infty}}{\omega_i/\omega - Y_{\mathrm{is}}}\right) = H_{\mathrm{Yi}} \ln\left(\frac{\omega_i/\omega - Y_{i\infty}}{\omega_i/\omega - Y_{\mathrm{is}}}\right) \tag{3}$$

where

$$H_{\mathrm{Yi}} = \left(\int_0^{y_\infty} \frac{1}{\rho D_i}\,\mathrm{d}y\right)^{-1} \tag{4}$$

This boundary-layer integration will need to be modeled and will be presented later. For convenience, two additional symbols are defined as

$$C_i = \frac{Y_{\mathrm{is}} - Y_{i\infty}}{\omega_i/\omega - Y_{\mathrm{is}}}, \qquad \zeta_i = \frac{\ln(1 + C_i)}{C_i} = \frac{\omega/H_{\mathrm{Yi}}}{\exp(\omega/H_{\mathrm{Yi}}) - 1} \tag{5}$$

Then Eq. (3) becomes

$$\omega = H_{\mathrm{Yi}} C_i \zeta_i \tag{6}$$

Finally, the vaporization rate of component i can be given by

$$\omega_i = H_{\mathrm{Yi}} \zeta_i C_i (\omega_i/\omega) = H_{\mathrm{Yi}} \zeta_i B_i \tag{7}$$

where

$$B_i = \frac{\omega_i}{\omega} C_i = \frac{Y_{\mathrm{is}} - Y_{i\infty}}{1 - Y_{\mathrm{is}}\omega/\omega_i} \tag{8}$$

It is the same as that of the droplet vaporization model except for the evaluation of H_{Yi}.

To obtain the expression for H_{Yi}, the Prandtl mixing-length theory[20] is applied. The viscosity is composed of a laminar component and a turbulent component. The laminar viscosity is the molecular viscosity, and the turbulent viscosity is proportional to the distance from the wall. The laminar component controls the diffusive transport in the region close to the film surface, whereas the turbulence component controls the diffusive transport in the region away from the wall, i.e., in the inertia sublayer region of the turbulent boundary layer. Thus H_{Yi} can be expressed as

$$H_{\mathrm{Yi}} = \begin{cases} \dfrac{\rho C_\mu^{\frac{1}{4}} K^{\frac{1}{2}}}{y_c^+ Sc_{\mathrm{Li}} + (Sc_T/\kappa)\ln\left(y^+/y_c^+\right)}, & y^+ > y_c^+ \\ \dfrac{\rho C_\mu^{\frac{1}{4}} K^{\frac{1}{2}}}{y^+ Sc_{\mathrm{Li}}}, & y^+ \le y_c^+ \end{cases} \tag{9}$$

where

$$y^+ = \rho C_\mu^{\frac{1}{4}} K^{\frac{1}{2}} y / \mu_L, \qquad y_c^+ = 11.5 \tag{10}$$

C. Description of the Liquid-Phase Submodel

Generally the flow inside the film is three-dimensional. For engine applications, however, the conductivity in the normal direction is much larger than that in other directions because of its thin thickness that is usually less than 100 μm. Also, the convective transport in the streamwise direction is accounted for by the Lagrangian description of the film particle method. Therefore, it is reasonable to assume that the film is quasi-one-dimensional in the normal direction, i.e., the variable distribution in the normal direction is independent of that in the streamwise direction. This is a good approximation for most of the film lifetime except during impingement. The governing equations for the film can be expressed as

$$\frac{\partial \rho \delta Y_i}{\delta \partial t} + \frac{\partial \rho Y_i (V_f + V_g)}{\delta \partial y^*} = \frac{\partial}{\delta^2 \partial y^*}\left(\Gamma \frac{\partial Y_i}{\partial y^*}\right)$$

$$\frac{\partial \rho \delta E}{\delta \partial t} + \frac{\partial \rho E (V_f + V_g)}{\delta \partial y^*} = \frac{\partial}{\delta^2 \partial y^*}\left(k \frac{\partial T}{\partial y^*}\right)$$

$$\text{I (convective)} \qquad \text{II (diffusion)} \tag{11}$$

where

$$y^* = y/\delta \tag{12}$$

V_f is used to account for the bulk velocity caused by the diffusion flux caused by incompressibility, and it is given by

$$\frac{\partial V_f}{\partial y} = \Sigma \frac{\partial}{\partial y} \frac{\Gamma}{\rho_i^0} \frac{\partial Y_i}{\partial y} \tag{13}$$

where ρ_i^0 is the density of pure component i. V_g is used to account for the film height change caused by vaporization, and it is expressed as

$$V_g = V_g^\delta y \big/ \delta \tag{14}$$

where V_g^δ is the surface regression rate. The film height h is evaluated using

$$\frac{\mathrm{d}\delta}{\mathrm{d}t} = V_g^\delta \tag{15}$$

At the interface continuity of the mass flux requires

$$\rho(V_g + V_f)|_{y=\delta} = \Sigma\, \omega_i \tag{16}$$

$$\Gamma \frac{\partial Y_i}{\partial y} = Y_i \Sigma\, \omega_i - \omega_i \tag{17}$$

Continuity of the heat flux gives

$$h_t(T_\infty - T_s) - k \left.\frac{\partial T}{\partial y}\right|_{y=\delta} = \Sigma\, \omega_i h_{\mathrm{vi}} \tag{18}$$

where h_t can be given by a modified wall function.[5] The other boundary conditions include

$$T = T_w, \qquad \frac{\partial Y_i}{\partial y} = 0, \qquad V_f = 0 \tag{19}$$

at the wall.

To obtain sufficiently accurate numerical solutions, tens of grid cells are required within the film. This is a tremendous computational cost. A more feasible predictive model is required.[5] The authors previously developed a model called the infinite-diffusion model.[17] It is an extension of the original O'Rourke and Amsden model[5] for single-component film vaporization. A piecewise linear distribution is used for temperature as the original O'Rourke and Amsden model. For mass fraction a uniform distribution is used. It requires the transient times for thermal diffusion and mass diffusion much less than the film lifetime (i.e., infinite diffusivity). Otherwise, its accuracy will become unacceptable. However, the transient times for fuel films in some practical applications can indeed be comparable to film lifetime as shown in the Appendix. Thus, a model that does not suffer from this restriction to small transient times is needed to model film vaporization accurately.

For thin films the convective term in Eq. (11) is smaller than the diffusion term and can be neglected. Consequently the governing equation for the temperature can be simplified as

$$\frac{\partial T}{\partial t} = \frac{\partial}{\partial y}\left(\alpha \frac{\partial T}{\partial y}\right) \tag{20}$$

where $\alpha = k/\rho Cp$, which is assumed to be constant along the y axis and is evaluated using average temperature and average mass fractions that vary with time.

A third-order polynomial expansion is used to model the temperature profile in the film at any instant

$$T = a_3(t)(y/\delta)^3 + a_2(t)(y/\delta)^2 + a_1(t)(y/\delta) + a_0(t) \tag{21}$$

where a_i can be expressed in terms of the wall temperature T_w, the average temperature T_m (defined by mass average), the surface temperature T_s, and the heat flux q to the film as

$$a_0 = T_w, \qquad a_1 = \beta\delta - 6T_s - 6T_w + 12T_m$$

$$a_2 = -3\beta\delta + 15T_s + 9T_w - 24T_m$$

$$a_3 = 2\beta\delta - 8T_s - 4T_w + 12T_m \tag{22}$$

where

$$\beta = q/k \tag{23}$$

Integration of Eq. (20) along the y axis yields

$$\frac{dT_m}{dt} = \frac{\alpha}{\delta^2}(6T_s + 6T_w - 12T_m) \tag{24}$$

Equation (20) expressed at the film surface yields

$$\frac{dT_s}{dt} = \alpha \left.\frac{\partial^2 T}{\partial y^2}\right|_{y=h} = \frac{6\alpha}{\delta^2}(\beta\delta - 3T_s - T_w + 4T_m) \tag{25}$$

Equation (25) has a nonphysical region. When the initial wall temperature is lower than the initial film temperature, the heat transfer to the wall will cause the decrease in the average and surface film temperatures. However, the surface temperature predicted by Eq. (25) initially increases for a short period and then decreases at later times because of aliasing errors on the polynomial expansion introduced by the step function between the initial wall and film temperatures. To overcome this problem, Eq. (25) is replaced by

$$\frac{dT_s}{dt} = \frac{6\alpha}{\delta^2}[\beta\delta + \min(0, -3T_s - T_w + 4T_m)] \tag{26}$$

When the wall temperature is higher than the initial temperature, Eq. (25) is replaced by

$$\frac{dT_s}{dt} = \frac{6\alpha}{\delta^2}[\beta\delta + \max(0, -3T_s - T_w + 4T_m)] \tag{27}$$

However, the preceding correction will not be needed when the computed temperature profiles become smooth.

By a similar approach as Eqs. (20–25), the equations for the average and surface mass fractions can be obtained. They are given by

$$\frac{dY_{is}}{dt} = \frac{\Gamma}{\rho\delta^2}(5\eta - 12Y_{is} + 12Y_{im}) \tag{28}$$

$$\frac{\partial Y_{im}}{\partial t} = \frac{\Gamma}{\rho\delta^2}\eta \tag{29}$$

where

$$\eta = (Y_i \Sigma w_i - w_i)\delta/\Gamma \tag{30}$$

The subtraction of Eq. (29) from Eq. (28) yields

$$\frac{d(Y_{is} - Y_{im})}{dt} = \frac{4\Gamma}{\rho\delta^2}[\eta - 3(Y_{is} - Y_{im})] \tag{31}$$

Equation (31) gives the difference between the surface and average mass fraction for component i. By using the overall mass balance equation to find the average mass fraction, Eq. (31) can be used to obtain the surface mass fraction needed to evaluate the vaporization rate.

D. Numerical Methods

The proposed models were implemented into a modified version[17] of KIVA-3V (Ref. 6). In the code the options of using the quasi-second-order-upwind differencing scheme or the partial-donor-cell (PDC) differencing scheme are available. The PDC scheme is used in this study to gain second-order accuracy spatially. The time-marching method is used, which consists of three steps. Step 1 deals with the coupling between sprays and gas-phase flow. Step 2 solves the gas flowfield with the Lagrangian method using the Euler implicit scheme (i. e., the grid moves with the flowfield). Step 3 adjusts the flowfield caused by grid movement using the Euler explicit scheme. The overall accuracy in time is of first-order accuracy.

Because the liquid-phase flow and the gas-phase flow are coupled at the interface, iterative approaches are used. The values (temperature and mass fractions) at the interface are estimated first, and then the computation of the liquid phase is made to check whether the continuity equations of mass and heat fluxes are satisfied. If they are not satisfied, the surface values are modified, and the liquid-phase computation is repeated until the continuity requirements are met. During this iteration process, the gas-phase parameters are taken from the preceding time step and held constant because the transient time of the gas boundary layer is, in general, longer than that of the liquid phase.

III. Results and Discussion

Two sets of computations were carried out to verify the accuracy and performance of the new model. The results are presented in the following sections.

A. Film Vaporization on a Semi-Infinite Flat Plate

Because there are little data available on film vaporization, an exact numerical solution for the film vaporization on a semi-infinite flat plate was used to verify the performance of the new model. The wall temperature is fixed at a constant value. Initially, the film temperature and the film height are uniform, and the ambient gas is nitrogen. For this particular problem the flows both inside and outside the film are one-dimensional in the direction normal to the wall. Therefore, they can be described by Eqs. (11–19). A finite difference method was used to solve these equations to obtain the exact numerical solution with the Euler-forward scheme in time and the central-difference scheme in space. A fine grid, which is uniform and consists of 100 cells with a grid size of 0.1 μm, and a small time step, 1e-2 ms, were used. The solutions obtained were independent of the grid size and the time step through successive grid and time-step refinement tests. This grid-independent exact numerical solution will be referred to as the exact solution in the following text. For comparison with the new model, the infinite-diffusion model[17] described in the preceding section was also applied.

1. *Accuracy of the Surface-Temperature Computations*

The transient heating process of a nonvaporizing film was first investigated to validate the correlation of Eqs. (25–27). The initial film temperature is uniform and higher than the wall temperature. At the interface there is a heat flux into the film from the ambient gas. For clarity this heat flux is artificially set to be constant during each computation. The film surface-temperature evolutions for different heat fluxes are shown in Fig. 1. The results are presented in the nondimensional form. The nondimensional time is defined as $\tau = tr_0^2/\alpha$, where α/r_0^2 is the characteristic time for thermal diffusion. The nondimensional temperature is depicted by temperature differences and given by $\theta = (T - T_0)/(T_0 - T_w)$. Figure 1a shows the results for the case with a heat flux $q = 0$. The result of the new model agrees very well with that of the exact numerical solution. The infinite diffusion model, however, underestimates the surface temperature initially and overestimates at later times. Eventually the three methods yield the same result when a steady state is reached. The result for $q = 0.1k(T_w - T_0)/\delta$ (low heat-flux case) and $q = k(T_w - T_0)/\delta$ (high heat-flux case) are shown in Figs. 1b and 1c, respectively. Clearly the new model gives better agreement

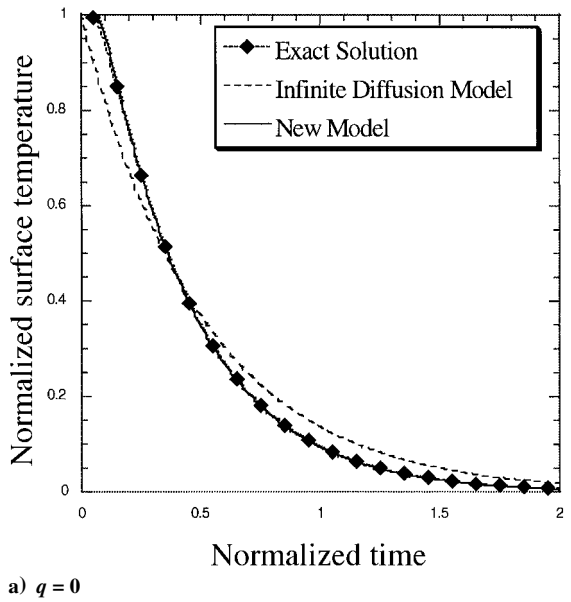

a) $q = 0$

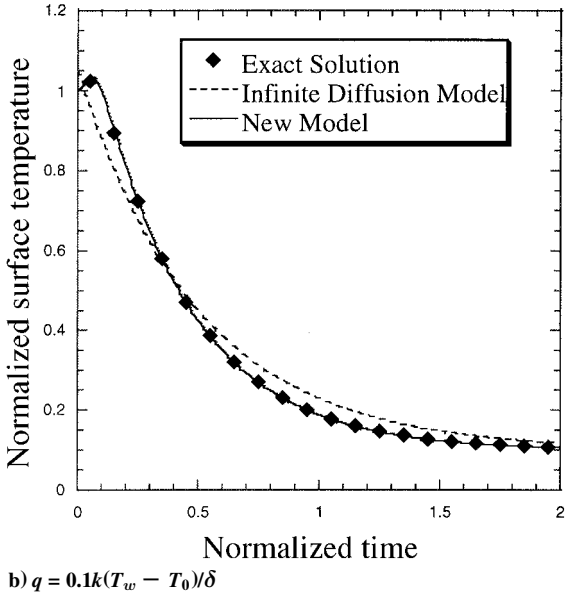

b) $q = 0.1k(T_w - T_0)/\delta$

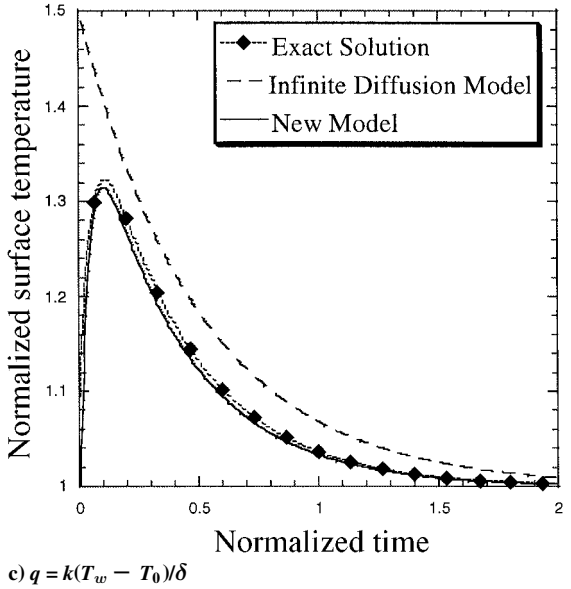

c) $q = k(T_w - T_0)/\delta$

Fig. 1 Normalized surface-temperature θ_s variation vs normalized time τ.

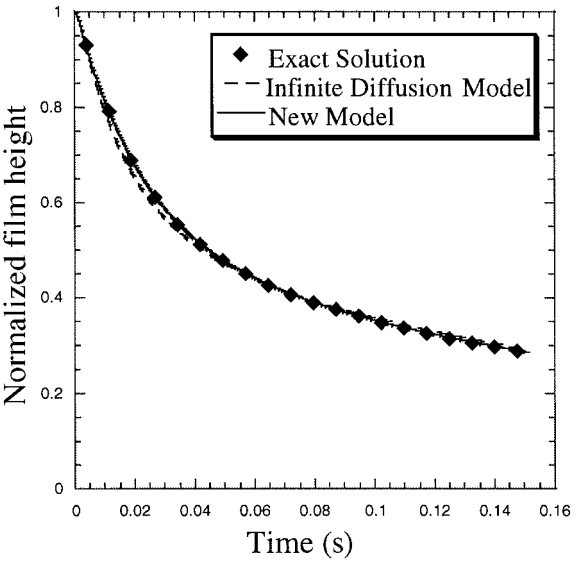

a) Normalized film-height δ/δ_0 variation vs time

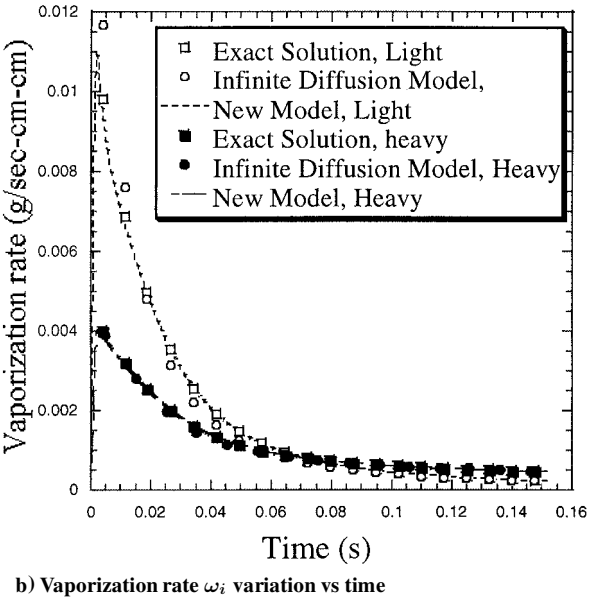

b) Vaporization rate ω_i variation vs time

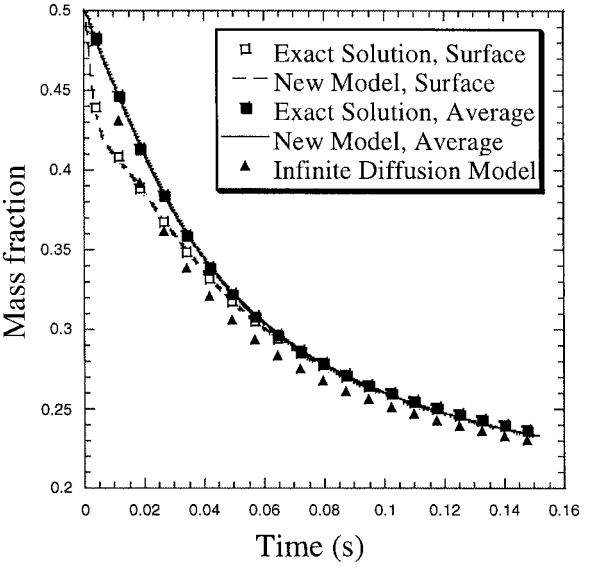

c) C_5H_{12} mass-fraction variation vs time

Fig. 2 Vaporization history of case A.

with the exact solution than the infinite-diffusion model. For the high heat-flux case the surface temperature initially increases for a period of time and then decreases at later times. The new model captures this trend very well and yields an accurate maximum surface temperature. In contrast, the infinite diffusion model does not show this trend and yields a much higher surface temperature initially that deviates from the exact solution by 50%. With the increased heat flux the accuracy of the infinite-diffusion model decreases while the accuracy of the new model remains the same. These results suggest that the new model is superior to the infinite-diffusion model for combustion applications, which typically feature high heat fluxes to the film.

2. Accuracy of the Multicomponent Computations

Three sets of computations were made to test the accuracy of the model for different vaporization rates and volatilities. In the first set of computation (case A), the film is composed of 50% C_5H_{12} and 50% C_6H_{14} by mass with an initial height δ_0 of 10 μm. The wall temperature is 320 K, while both the initial film temperature and the ambient gas temperature are 293.15 K. The ambient gas is quiescent, and the initial turbulent intensity is set near zero, so that the gas flow is basically laminar. Figure 2a shows the computed normalized film height δ/δ_0 variation vs time, Fig. 2b shows the variations of the component vaporization rate ω_i, and Fig. 2c shows the variations of the mass fraction of C_5H_{12}. The three methods yield similar results because of the slow vaporization rate. Equation (31) shows that the difference between the surface mass fraction and the average mass fraction is proportional to the vaporization rate. Because this difference in this case is very small, the mass-fraction distribution is nearly uniform, and the two models yield similar results that agree well with those of the exact numerical solution. However, if the vaporization rate is not small, the difference between the models becomes apparent. In terms of CPU time, the exact numerical solution takes much longer than the infinite-diffusion model or the present model by nearly 100 times because 100 grid cells are used and much more iterative steps are needed for liquid-phase computation in the exact numerical solution during each time step.

In the second set of computations (case B), all of the parameters were the same as those in case A except for the diffusivity in the gas phase. The diffusivity was increased by 20 times to simulate

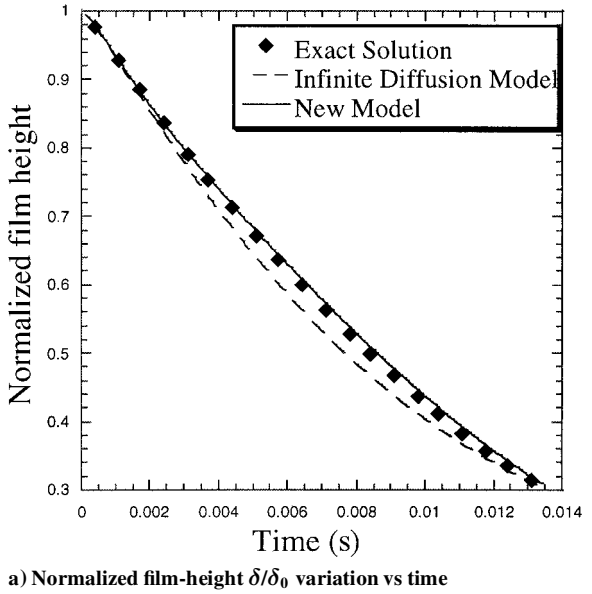

a) Normalized film-height δ/δ_0 variation vs time

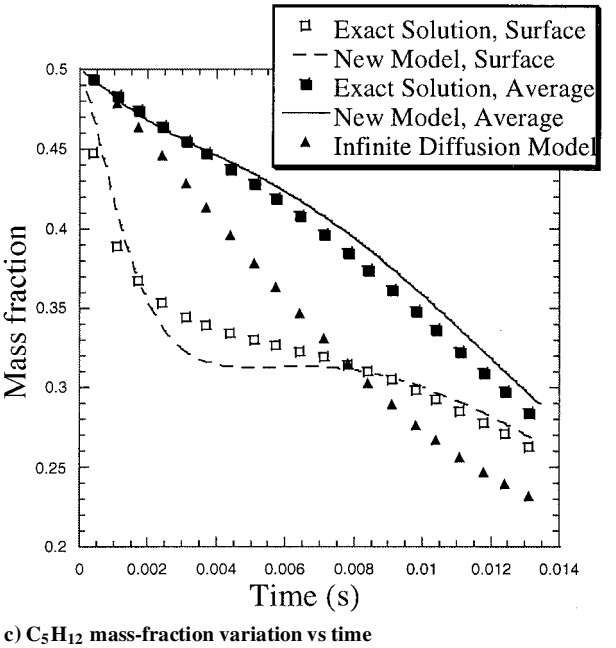

c) C_5H_{12} mass-fraction variation vs time

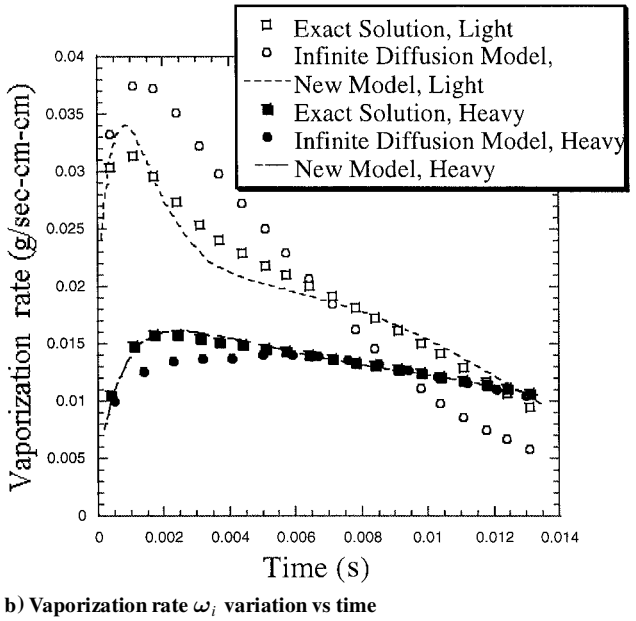

b) Vaporization rate ω_i variation vs time

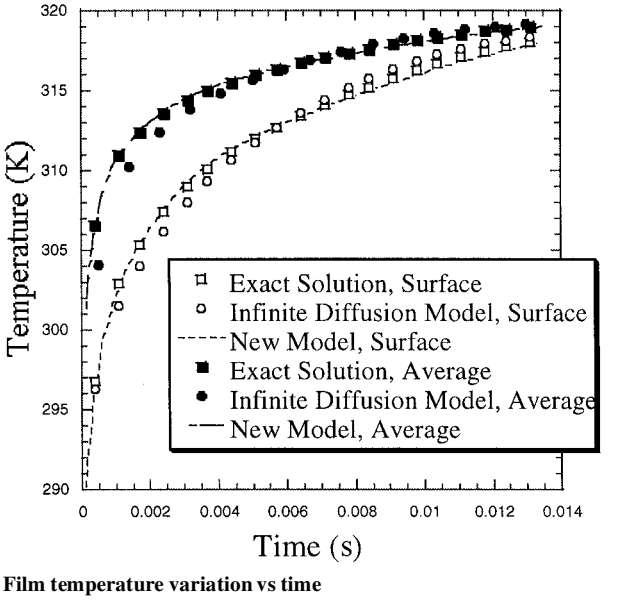

d) Film temperature variation vs time

Fig. 3 Vaporization history of case B.

the enhancement of the diffusive transport of mass and energy by turbulence. In effect the vaporization rate is increased by nearly 20 times. The computed variations vs time in normalized film height δ/δ_0, vaporization rate ω_i, and mass fraction of C_5H_{12} are shown in Fig. 3. The three methods predict similar lifetimes for the film although the infinite-diffusion model results in a slightly longer lifetime. However, the infinite-diffusion model overestimates the vaporization rate of the light component and underestimates that of the heavy component (Fig. 3b). In contrast, the results of the new model agree reasonably well with those of the exact solution because of the effect of preferiential vaporization. Because of the mass-diffusion resistance inside the film, the mass fraction inside cannot quickly reach the surface where the vaporization occurs. This results in the surface mass fraction of the light component being lower than the average mass fraction as shown in Fig. 3c. Figure 3d gives the variations of the surface and average temperatures vs time, and it shows that the infinite diffusion model underestimates both the surface and average temperatures.

Fuel consisting of 50% C_5H_{12} and 50% $C_{10}H_{22}$ by mass was used in the third set to show the effects of the volatility (case C). The other parameters are the same as those of case B. The variation vs time in normalized film height δ/δ_0 and mass fraction of C_5H_{12} is shown in Fig. 4. Compared to case B, the volatility difference between components in this case is much larger. The new model offers better agreement with the exact solution than the infinite-diffusion model in this case as well, which indicates that the new model is suitable for fuel composed of components with large volatility difference.

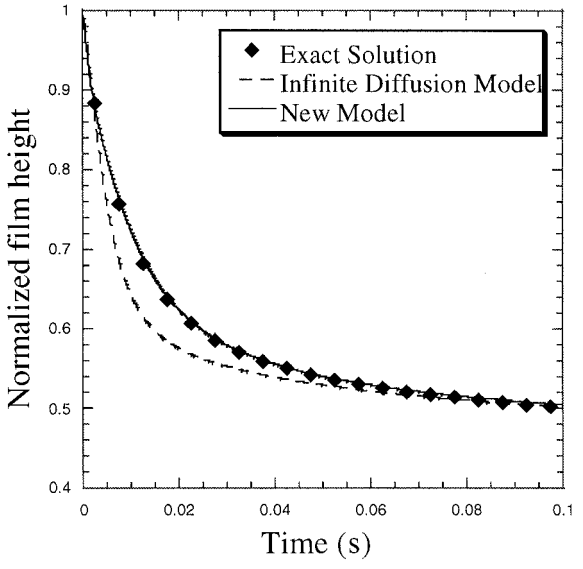

a) Normalized film-height δ/δ_0 variation vs time

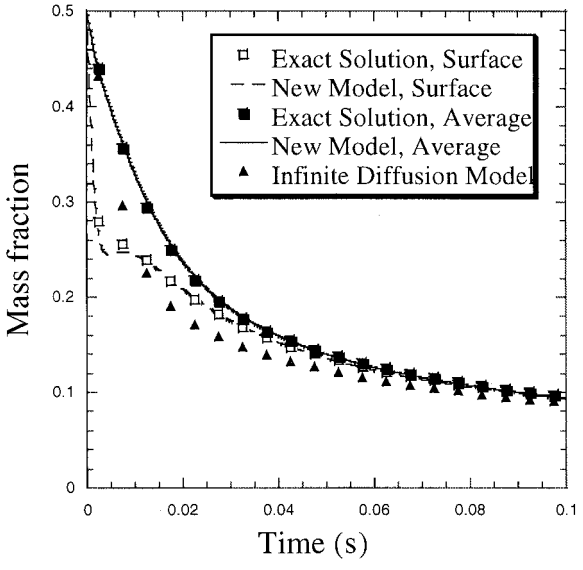

b) C_5H_{12} mass-fraction variation vs time

Fig. 4 Vaporization history of case C.

B. Film Formation and Evolution During Spray/Wall Impingement Process

The new model was used to predict the film formation and evolution during spray impingement on a wall. The injection data were chosen to match a typical injection cycle in a port-injected spark-ignition engine. The fuel used in the computation consisted of 50% C_5H_{12} and 50% C_6H_{14} by mass same as those used in cases A and B. The injection parameters and the ambient parameters used are listed in Tables 1 and 2. The injection velocity was chosen to ensure that some of the droplets became part of the film. The splash model of Trujillo et al.[10] was used in this study. The three-dimensional mesh consisted of $40 \times 30 \times 30$ cells in the streamwise, normal, and transverse directions, respectively, with higher resolution in the impingement region. Three-thousand parcels were used to represent the spray. The time step was decided by numerical stability analysis.

Figure 5 shows the plot of droplet locations with the symbol size representing the particle mass at $t = 1.3$ ms shortly after the impingement. The beginning of the impingement corresponds to $t = 1.2$ ms. The impingement duration was approximately 4 ms. Nearly 30% of the droplets became part of the wall films, and the rest splashed and became smaller secondary droplets. The contour plot of C_5H_{12} vapor density at $t = 6$ ms after the beginning to the impingement is shown in Fig. 6 (the ratio of height to wide is enlarged by 10 times). The fuel vapor density evolution in the boundary layer was observed downstream of the impingement point. The wall particles move downstream under the influence of the main flow above the film. The evolutions of the total liquid fuel mass (including both droplets and films) and the film mass are plotted in Fig. 7. For the total liquid fuel mass four distinct phases were observed. At phase I the fuel mass increases linearly with time because of the injection rate being much higher than the vaporization rate. Phase II starts after the end of injection and ends after the beginning of the impingement with short delay. During this phase, the liquid mass

Table 1 Injection parameters

Parameter	Value
Injected mass	2.34 mg
Injection velocity	25 m/s
Spray cone angle	10 deg
Injection duration	1.1 ms
Sauter mean diameter	30 μm
Impingement angle	45 deg

Table 2 Ambient parameters

Parameter	Value
Gas temperature	353 K
Gas velocity	50 m/s
Gas compostition	N_2
Wall temperature	315 K
Gas pressure	1 atm

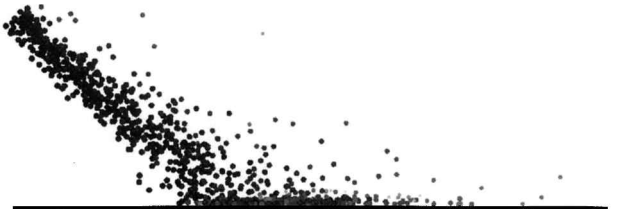

Fig. 5 Plot of droplet position.

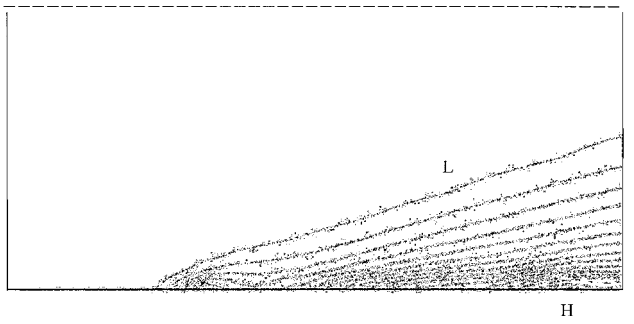

Fig. 6 Plot of C_5H_{12} vapor contour line (the ratio of height to width is enlarged by 10 times) ($H = 1 \times 10^{-3}$ g/cm^3, $L = 0$ g/cm^3, contour increment = 5×10^{-5} g/cm^3).

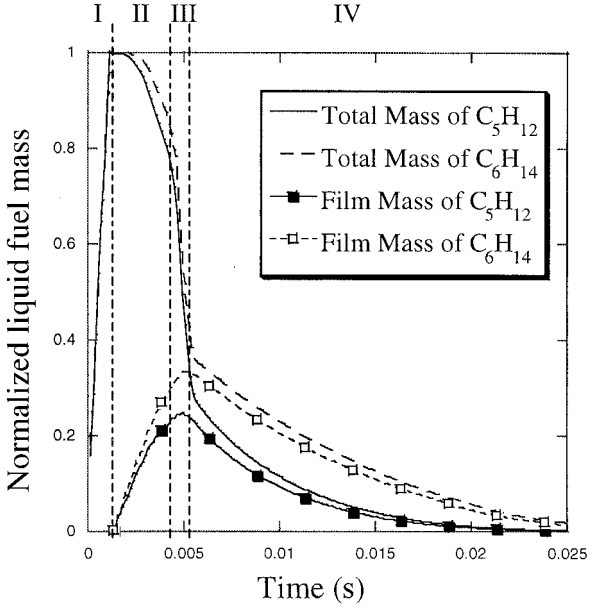

Fig. 7 Film and total liquid fuel mass variation vs time.

begins to decrease and vary nearly linearly with time because of the nearly constant overall droplet vaporization rate. Phase III lasts until all of the droplets not on the wall completely vaporize. The duration of this phase is much shorter compared to phase II. In addition, this phase has a higher vaporization rate, which is caused by the splashing. The splashing causes injected droplets to break up into smaller droplets, which result in more surface area for vaporization. Phase IV was dominated by the vaporization of wall films. Clearly the reduction rate of the liquid mass is much slower than that of phase II and phase III. The film vaporization rate decreases with increasing time because of fuel vapor accumulation in the region near the film surface as shown in Fig. 7. It is interesting that film particles, which account for nearly 30% of total fuel mass, take 20 ms to vaporize completely, whereas the rest that accounts for nearly 70% of the total mass takes only less than 5 ms. This is part of the reason why open-valve injection results in higher hydrocarbon emission in a port-injected engine than closed-valve injection. Open-valve injection tends to have more droplets impingement on the in-cylinder wall and more liquid film accumulated in the cylinder. Because the vaporization rate of the films is much slower than that of droplets as demonstrated in Fig. 7, the fuel films do not vaporize completely during the compression stroke and eventually contribute to higher hydrocarbon emissions. Figure 8 shows a comparison of the predicted-film mass-temporal variations for the new model and the infinite-diffusion model. The two models give similar film lifetimes. However, the film mass predicted by the infinite-diffusion model deviates from that of the new model by 20%.

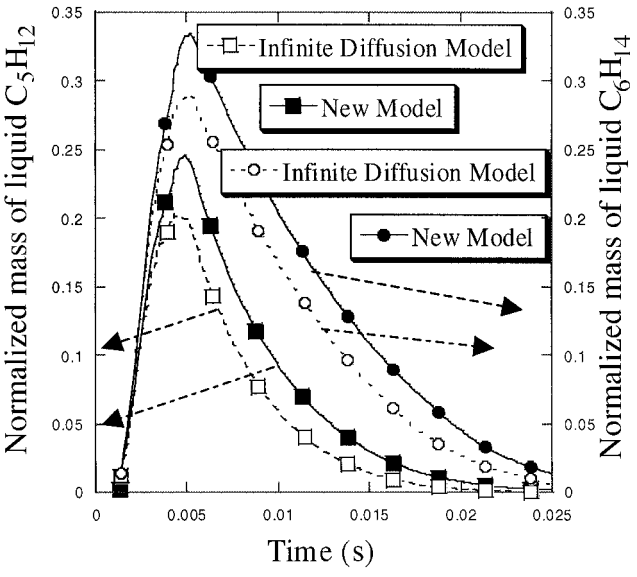

Fig. 8 Comparison of the film mass evolution of two models.

IV. Conclusions

A new vaporization model for multicomponent films has been developed and verified through extensive comparisons. The model consists of the coupling of the gas-phase and liquid-phase submodels. The gas-phase submodel accounts for the multicomponent fuel effects on the mass and energy transports of the gas turbulent boundary layer above the liquid film. The effects of the temperature and concentration gradients caused by nonuniformity inside the liquid film are represented in the liquid-phase submodel. A third-order polynomial is used to simulate the temperature and mass-fraction profiles, and the governing equations for the mass and energy transports are reduced to a set of ordinary differential equations. The primary benefit of this model is a tremendous decrease in computational cost, with only a minor loss of accuracy compared to solving directly the strict governing equations for the film. The results of the tests and comparisons can be summarized as follows:

1) The liquid-phase model, which is the foundation of the new model, yields excellent agreement between the surface temperatures predicted by the model and those of the exact numerical solution for a nonvaporizing film regardless of the magnitude of the heat flux to the film. However, the infinite-diffusion model, which assumes the temperature profile being piecewise linear and the concentration distribution of each component being uniform, can give a sufficiently accurate surface temperature only when the heat flux is small.

2) The computed vaporization history of a multicomponent film on a semi-infinite flat plate agrees well with the exact solutions. There are significant differences in the vaporization rate, temperature, and concentration predicted by the new model vs those by the infinite-diffusion model when the transient time of the mass-diffusion transport is comparable to the film lifetime.

3) The overall film lifetime is not sensitive to the liquid-phase model. The infinite-diffusion model yields vaporization rates that are slower initially and higher at later times compared to the new model and the exact numerical solution. Nevertheless, it predicts an overall film lifetime similar to the new model and the exact solution.

4) For the vaporization of a spray impinging on a wall, four distinctive phases were found in the evolution of the liquid fuel mass. The droplet splashing enhanced fuel vaporization, whereas the conversion into wall films slowed down fuel vaporization significantly.

5) The low computational cost and the good accuracy of the new model make it particularly suitable for multidimensional spray and combustion computations. The accuracy of the model is much better than that of the infinite-diffusion model, whereas its computational cost is only slightly more than that of the infinite-diffusion model.

Appendix: Estimation of Film Lifetime

In this session the formulas to estimate the film vaporization rate and the film lifetime are presented. They are based on the analyses of a thin film composed of a single-component fuel on a semi-infinite flat plate of a constant and uniform temperature.

If the vaporization rate is very slow, the film temperature can be assumed constant. Then the governing equation for the vapor mass fraction outside the film becomes similar to that of the thermal conduction problem over a semi-infinite flat plate, where the heat flux on the wall is given by

$$q = k \left.\frac{\partial T}{\partial y}\right|_{y=0} = k\frac{T_\infty - T_w}{\sqrt{\pi \alpha t}} \tag{A1}$$

where k is the heat conductivity, α is the thermal diffusivity, and T_w and T_∞ are temperatures at the wall and at infinity, respectively. Similarly, the mass flux (vaporization rate) on the film surface can by given by

$$\omega = \frac{D\partial Y/\partial y|_{y=0}}{1 - Y_w} = \frac{D(Y_\infty - Y_w)}{\sqrt{\pi Dt}(1 - Y_w)} = \sqrt{\frac{D}{\pi t}}B \tag{A2}$$

where B is the transfer number and D is the mass-diffusion coefficient. Y_0 and Y_∞ are the vapor mass fractions at the wall and at infinity, respectively. When the vaporization rate is high, the blowing factor can be used to consider the influence of vaporization on mass diffusion. Thus, the vaporization rate can be roughly given by

$$\omega = \sqrt{\frac{D}{\pi t}}B\frac{\ell n(1 + B)}{B} = \sqrt{\frac{D}{\pi t}}\ell n(1 + B) \tag{A3}$$

Figure A1 gives the comparison between the solution by Eq. (A3) and by an exact numerical solution for this problem. The two solutions are fairly close with the same order of magnitude. Then the lifetime scale of film can be given by

$$t_v = \frac{\pi}{4}\left(\frac{\rho_\ell}{\rho_g}\right)^2 \frac{h^2}{D}\left[\frac{1}{\ell n(1 + B)}\right]^2 \tag{A4}$$

ρ_g and ρ_ℓ are the fuel densities of the gas phase and the liquid phase. The thermal transient time of the film can be given by

$$t_f = h^2/\alpha_\ell \tag{A5}$$

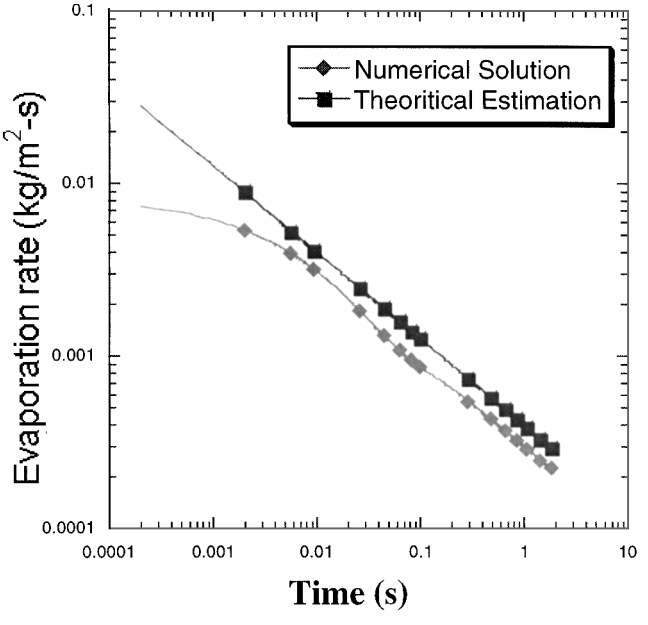

Fig. A1 Comparison between the theoretically estimated and numerically computed vaporization rates.

where α_ℓ is the thermal diffusivity of the liquid phase. For a film composed of Pentane at 293.15 K and 1 atm, if the gas-phase flow outside the film is laminar the ratio of the transient time to the film lifetime is

$$\frac{t_f}{t_v} = \frac{4}{\pi}\left(\frac{\rho_g}{\rho_\ell}\right)^2 \frac{D}{\alpha_\ell}[\ell n(1 + B)]^2 \cong 0.0256 \tag{A6}$$

The thermal transient time only accounts 2% of the film lifetime. If we consider the enhancement of the thermal diffusion transport by turbulence in the gas phase, the vaporization lifetime scale t_v will become much shorter. If we simply assume that the gas mass diffusivity is enlarged by 20 times, the lifetime scale will become comparable to thermal transient time. Moreover, for mass diffusion because the liquid mass diffusivity is much smaller than the liquid thermal diffusivity, the ratio will be larger. Typically it is larger by 10 times because the Lewis number is on the order to 10. Therefore, the transient process inside the film must be considered for the cases with highly volatile fuel and turbulent gas flow. These cases are frequently seen in the industrial applications.

Acknowledgments

This work was supported in part by the National Science Foundation under Grant CTS-9734402, with Farley Fisher as Technical Monitor, and by Ford Motor Company, with Eric Curtis as Technical Monitor. We also thank Dar-Lon Chang and Yu-Yu Lee for their assistance on preparing the manuscript.

References

[1]Zeng, Y., and Lee, C. F., "Modeling of Multicomponent Fuel Spray and Film Evaporations in I.C. Engines," *Proceedings of the 2nd Asia-Pacific Conference on Combustion*, May 1999, pp. 186–189.

[2]Min, K-D., and Norris, M., "An Overview of Hydrocarbon Emissions Mechanisms in Spark-Ignition Engines," Society of Automotive Engineers, Paper 932078, 1993.

[3]Shin, Y., Cheng, W. K., and Heywood, J. B., "Liquid Gasoline Behavior in the Engine Cylinder of an SI Engine," Society of Automotive Engineers, Paper 941872, 1994.

[4]Gallopoulus, N., "Bridging the Present to the Future in Personal Transportation—The Role of Internal Combustion Engines," Society of Automotive Engineers, Paper 920721, 1992.

[5]O'Rourke, P. J., and Amsden, A. A., "A Particle Numerical Model for Wall Film Dynamics in Port-Injected Engines," Society of Automotive Engineers, Paper 961961, 1996.

[6]Amsden, A., "KIVA-3V: A Block-Structured KIVA Program for Engines with Vertical or Canted Valves," Los Alamos National Lab. Rept. LA-13313-MS, Los Alamos, NM, 1997.

[7]Bai, C., and Gosman, A. D., "Mathematical Modeling of Wall Films Formed by Impinging Sprays," Society of Automotive Engineers, Paper 960626, 1996.

[8]Foucart, H., Habchi, C., Le Coz, J. F., and Baritaud, T., "Development of a Three Dimensional Model of Wall Fuel Liquid Film for Internal Combustion Engines," Society of Automotive Engineers, Paper 980133, 1998.

[9]Nagaoka, M., Kawazoe, H., and Nomura, N., "Modeling Fuel Spray Impingement on a Hot Wall for Gasoline Engines," Society of Automotive Engineers, Paper 940525, 1994.

[10]Trujillo, M. F., Mathews, W. S., Lee, C. F., and Peters, J. E., "A Computational and Experimental Investigation of Spray/Wall Impingement," *Proceedings of the ILASS Americas 11th Annual Conference on Liquid Atomization and Spray Systems*, May 1998, pp. 111–114.

[11]Baumann, W. W., and Thiele, F., "Heat and Mass Transfer in Evaporating Two-Component Liquid Flow," *International Journal of Heat and Mass Transfer*, Vol. 33, No. 2, 1990, pp. 267–273.

[12]Baumann, W. W., and Thiele, F., "Effect of Phase Equlibrium on the Interfacial Transfer Behavior in Evaporating Two-Component Liquid Film Flow," *Advances in Gas-Liquid Flows*, American Society of Mechanical Engineers, FED, New York, 1990, pp. 389–396.

[13]Suzuki, K., Hagiwara, Y., and Sato, T., "Heat Transfer and Flow Characteristics of Two-Phase Two-Component Annular Flow," *International Journal of Heat and Mass Transfer*, Vol. 26, No. 4, 1983, pp. 597–605.

[14]Shembharkar, T. R., and Pai, B. R., "Prediction of Film Cooling with a Liquid Coolant," *International Journal of Heat and Mass Transfer*, Vol. 29, No. 6, 1986, pp. 899–908.

[15]Chow, L. C., and Chung, J. N., "Evaporation of Water into a Laminar Stream of Air and Superheated Steam," *International Journal of Heat and Mass Transfer*, Vol. 26, No. 3, 1983, pp. 373–380.

[16]Yan, W., "Effects of Film Evaporation on Laminar Mixed Convection Heat and Mass Transfer in a Vertical Channel," *International Journal of Heat and Mass Transfer*, Vol. 35, No. 12, 1992, pp. 3419–3429.

[17]Zeng, Y., and Lee, C. F., "Computations of In-Cylinder Multicomponent Fuel Distribution of a Port Injected Spark Ignition Engine," *Proceedings of the ILASS Americas 11th Annual Conference on Liquid Atomization and Spray Systems*, May 1998, pp. 96–100.

[18]Ayoub, N. S., and Reitz, R. D., "Multidimensional Computation of Multicomponent Spray Vaporization and Combustion," Society of Automotive Engineers, Paper 950285, 1995.

[19]Abraham, J., and Magi, V., "A Model for Multicomponent Droplet Vaporization in Sprays," Society of Automotive Engineers, Paper 980511, 1998.

[20]Launder, B. E., and Spalding, B. E., "The Numerical Computations of Turbulent Flows," *Computer Methods in Applied Mechanics and Engineering*, Vol. 3, No. 2, 1974, pp. 269–289.